IAA-AAS-DyCoSS2-03-04

OPTIMISATION OF SOLAR SAIL INTERPLANETARY HETEROCLINIC CONNECTIONS

Jeannette Heiligers,[†] Giorgio Mingotti,[‡] and Colin McInnes[§]

This paper investigates time-optimal solar sail trajectories between displaced Libration Point Orbits (LPOs) of different circular restricted three-body systems. Key in the investigations is the search for transfers that require little steering effort to enable the transfers with low control authority solar sail-like devices such as SpaceChips. Two transfers are considered: 1) from an Earth-L_2 Halo orbit to a Mars-L_1 Halo orbit and 2) from an Earth-L_1 Halo orbit to a Mercury-L_2 Halo orbit. For both transfers the optimal control problem is derived and solved with a direct pseudospectral method. For a sail performance comparable to that of NASA's Sunjammer sail, the results show transfers that require very little steering effort: the sail acceleration vector can be bounded to a cone with a half angle of 5 deg (Earth-Mars) or even 2.5 deg (Earth-Mercury). These transfers can serve a range of novel solar sail applications covering the entire spectrum of sail length-scales: micro-sized SpaceChips could establish a continuous Earth-Mars communication link, a traditional-sized sail provides opportunities for in-situ observations of Mercury and a future kilometer-sized sail could create an Earth-Mars cargo transport gateway for human exploration of Mars.

INTRODUCTION

Research in the field of solar sailing is flourishing, sparked by successes such as JAXA's IKAROS mission [1] and new solar sail initiatives including NASA's Sunjammer mission. [2] Its potential lies in the fact that solar sail missions are not constrained by a propellant mass: [3] by using the Sun as "propellant source", solar sails obtain their propulsive acceleration by reflecting photons off a highly reflective membrane. This gives solar sails a theoretically unlimited lifetime and enables a wealth of novel orbits and space applications, including displaced geostationary orbits to create additional geostationary slots for telecommunication, Earth observation and

[†] Research Associate, Advanced Space Concepts Laboratory, Department of Mechanical & Aerospace Engineering, University of Strathclyde, 75 Montrose Street, G1 1XJ Glasgow, U.K. e-mail: jeannette.heiligers@strath.ac.uk.
[‡] Research Associate, Advanced Space Concepts Laboratory, Department of Mechanical & Aerospace Engineering, University of Strathclyde, 75 Montrose Street, G1 1XJ Glasgow, U.K. e-mail: giorgio.mingotti@strath.ac.uk.
[§] Professor, Advanced Space Concepts Laboratory, Department of Mechanical & Aerospace Engineering, University of Strathclyde, 75 Montrose Street, G1 1XJ Glasgow, United Kingdom. e-mail: colin.mcinnes@strath.ac.uk.

weather satellites [4, 5] and orbits displaced below the lunar south pole [6] or above the Earth-Moon L_2 point [7] to establish an Earth-Moon communications link.

Instead of investigating the set of novel orbits that solar sails enable, this paper focusses on their transfer capabilities, in particular in the circular restricted three body problem (CR3BP). Solar sail transfers in the CR3BP have been investigated before, for example to fly out to periodic orbits around Lagrange points (also referred to as Libration Point Orbits (LPOs)) [8] and to move between artificial equilibrium points [9]. However, solar sail transfers between LPOs in *different* three-body systems have so-far not been investigated, despite the fact that they offer great potential for additional novel space applications. Note that these types of interplanetary heteroclinic connections have been the topic of a limited number of papers [10-12], but all considered either the use of an impulsive maneuver to establish the connection or the use of solar electric propulsion, while this paper demonstrates the capabilities of solar sailing.

For the purpose of demonstrating the concept's feasibility, this paper investigates two particular solar sail transfers: 1) the transfer from an Earth-L_2 Halo orbit to a Mars-L_1 Halo orbit and 2) the transfer from an Earth-L_1 Halo orbit to a Mercury-L_2 Halo orbit. For both cases the time-optimal transfer will be sought for by solving the accompanying optimal control problem with a direct pseudospectral method. Note that, while *solar sail displaced* LPOs exist [13], this work only considers the transfer between LPOs in the classical CR3BP. The solar sail acceleration is thus only employed to leave and wind onto the Halo orbits.

Another novelty introduced in this paper is the consideration of low control authority solar sails that can change their attitude only to a limited extent. The reason for investigating this scenario is the development of so-called SpaceChips: miniturised operational spacecraft of a few centimeters in size. With a high area-to-mass ratio, these devices act as solar sails and with low production costs and low mass they enable a range of new space applications [14], but will have limited steering capabilities. Constraints on the control authority of solar sails have been investigated before. For example, in Reference [15] time-optimal Earth-Mars orbital rendezvous missions were found after fixing the cone angle. However, with still full control over the clock angle and relatively large (constant) cone angles, significant control authority can still be achieved. Instead, in this work the authors show that even with extremely low control authority feasible and relatively quick transfers can be accomplished.

For comparison and to highlight the difference applications of the transfers, this paper will consider both high control authority traditional solar sails as well as control limited SpaceChips. Distributing micro-sized (10^{-2} m), low control authority SpaceChips along a trajectory connecting an Earth L_2-orbit with an L_1-orbit at Mars establishes a continuous Earth-Mars communication link, even during Martian occultation; alternatively, a meso-sized (10-100 m), fully steerable solar sail can enable an interesting planetary observation platform at Mercury through the use of a connection between Earth-L_1 and Mercury-L_2; and finally, in the macro-scale (10^3 m), the previously mentioned Earth-Mars link allows a vital gateway for cargo transport for future human exploration on Mars.

The structure of the paper will be as follows. First, the dynamical model will be explained: the classical circular restricted three body problem will be revisited and a solar sail acceleration will be added. To include fourth body perturbations the ephemerides employed will be described and the required reference frame transformations are discussed. Finally, the LPOs considered in this paper will be derived and presented. The second part of the paper will focus on the definition of the optimal control problem. Since the start and end points of the transfer are defined in different CR3BPs, a two phased approach will be introduced. The required phase-linkage constraints, boundary constraints and path constraints will be discussed. The latter include the important con-

straint on the steering capability of the solar sail in order to mimic the low control authority of SpaceChips. Subsequently the optimal control solver and initial guesses are introduced. The last part of the paper will present the results for both the Earth-to-Mars and Earth-to-Mercury transfers and the paper will end with the conclusions.

DYNAMICAL MODEL

Circular restricted three-body problem

The dynamic model employed in this paper is the well-known circular restricted three-body problem (CR3BP), which describes the motion of an infinitely small mass, m, (here the solar sail) under the influence of the gravitational attraction of two much larger masses, m_1 and m_2, also referred to as the primaries. The gravitational influence of the small mass on the primaries is neglected and the primaries are assumed to move in circular orbits about their common centre-of-mass. [16]

The reference frame employed is a synodic reference frame and is depicted in Figure 1: the origin coincides with the barycentre of the system, the x-axis connects m_1 and m_2 and points in the direction of m_2, the z-axis is directed perpendicular to the plane in which m_1 and m_2 orbit and the y-axis completes the right-handed reference frame. Finally, the frame rotates at constant angular velocity, ω, around the z-axis: $\boldsymbol{\omega} = \omega \hat{\mathbf{z}}$.

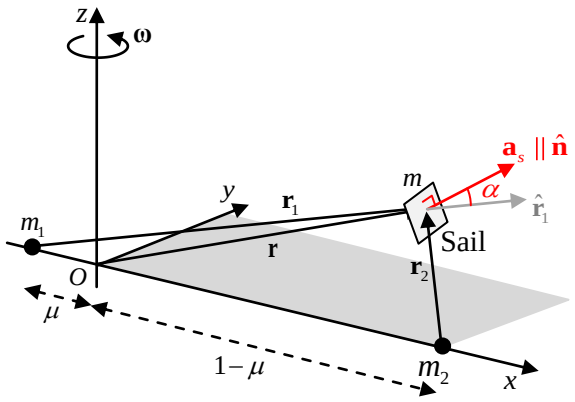

Figure 1 Schematic of circular restricted three-body problem.

New units are introduced in the CR3BP: the sum of the two larger masses is taken as the unit of mass, i.e. $m_1 + m_2 = 1$. Then, with the mass ratio $\mu = m_2 / (m_1 + m_2)$, the masses of the primaries become $m_1 = 1 - \mu$ and $m_2 = \mu$. As unit of length, λ, the distance between the primaries is selected, and $1/\omega$ is chosen as unit of time, τ, yielding $\omega = 1$, and so one orbital period of the planet around the Sun is represented by 2π.

Three different CR3BPs will be employed throughout this work: Sun-Earth, Sun-Mars and Sun-Mercury. Parameters for each of the CR3BPs are provided in Table 1.

The motion of a solar sail in any of these CR3BPs is governed by the following equations of motion: [3]

$$\ddot{\mathbf{r}} + 2\boldsymbol{\omega}\times\dot{\mathbf{r}} + \boldsymbol{\omega}\times\left(\boldsymbol{\omega}\times\mathbf{r}\right) + \nabla V = \mathbf{a}_s + \mathbf{a}_4 \tag{1}$$

with V the gravitational potential and nearly all other definitions provided in Figure 1. The left hand side of Eq. (1) describes the classical (i.e. ballistic) CR3BP, while the right hand side adds two perturbing terms: the solar sail acceleration, $\mathbf{a}_s$, and the fourth body perturbation $\mathbf{a}_4$, which will be discussed in the next two subsections.

Table 1 Circular restricted three-body problem parameters

CR3BP	μ	λ	τ	μ_4
Sun-Earth	3.0034599e-6	1.4947600e9	5.0162789e6	Mercury: 1.6601428e-7 Mars: 3.2268266e-7
Sun-Mars	3.2268352e-7	2.2793910e9	9.4461038e6	Earth: 3.0034679e-6
Sun-Mercury	1.6601475e-7	5.7909100e7	1.2096630e6	Earth: 3.0034684e-6

Solar sail acceleration

An ideal solar sail model is adopted, which assumes pure specular reflection of the impinging photons. [3] The solar sail acceleration vector then acts along the normal vector to the solar sail surface, i.e. in direction $\hat{\mathbf{n}}$, and is defined as:

$$\mathbf{a}_s = \beta\frac{1-\mu}{r_1^2}\left(\hat{\mathbf{r}}_1\cdot\hat{\mathbf{n}}\right)^2\hat{\mathbf{n}} \tag{2}$$

From Eq. (2) it is clear that the sail acceleration magnitude is proportional to the solar gravitational acceleration, $(1-\mu)/r_1^2$, and is scaled by the sail lightness number, β. The lightness number can be expressed as a function of the sail area to spacecraft mass ratio, σ, and the critical solar sail loading parameter, $\sigma^* = 1.53$ g/m^2: [3]

$$\beta = \frac{\sigma^*}{\sigma} \tag{3}$$

A realistic near-term value for the lightness number can be derived from the expected lightness number of the Sunjammer mission which is in the range 0.0388-0.0455. For convenience, this work will consider the top-end of this range and select a value of $\beta = 0.05$. Another common parameter to express the performance of a solar sail is the characteristic acceleration, which is defined as the acceleration produced by a Sun-facing solar sail at Earth's distance. A sail lightness number of 0.05 thus corresponds to a characteristic acceleration $a_c = \beta\frac{\mu_S}{\mathrm{AU}^2} = 0.3$ mm/s^2 with μ_S the gravitational parameter of the Sun and AU the astronomical unit.

Finally, Eq. (2) takes into account the reduced projected solar sail area when the sail is pitched at a cone angle, $\alpha = \cos^{-1}\left(\hat{\mathbf{r}}_1 \cdot \hat{\mathbf{n}}\right)$, with respect to the Sun-sail line through the term $\left(\hat{\mathbf{r}}_1 \cdot \hat{\mathbf{n}}\right)^2$, see also Figure 1.

Fourth body perturbation

As became clear in the introduction, the starting LPO and target LPO are defined in different CR3BPs. The first and second sections of the transfer connecting these LPOs will therefore also be defined in different CR3BPs. In order for the dynamics to be consistent throughout the transfer, a fourth body perturbation is included. For example, for the Earth-L_2 to Mars-L_1 transfer, Mars will be the fourth body in the Sun-Earth CR3BP, while the Earth will be the fourth body in the Sun-Mars CR3BP.

The perturbing acceleration, $\mathbf{a}_4$, is defined as: [10]

$$\mathbf{a}_4 = \frac{\partial \Omega_4}{\partial \mathbf{r}}, \quad \Omega_4 = \frac{\mu_4}{r_4} - \frac{\mu_4}{\rho_4^2}\left(x\cos\theta_4 + y\sin\theta_4\right) \tag{4}$$

with $\mu_4 = m_4/\left(m_1 + m_2\right)$ and m_4 the mass of the fourth body, see Table 1 for values. All other variables in Eq. (4) are defined in Figure 2.

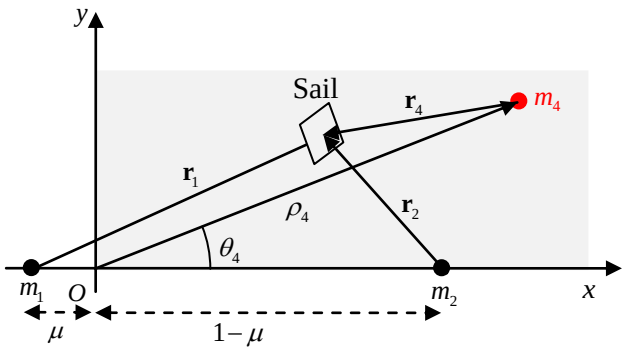

Figure 2 Fourth body perturbation geometry.

Ephemerides

The inclusion of the fourth body perturbation transforms the autonomous CR3BP into a non-autonomous problem through the angle θ_4. The actual relative position of the planets thus comes into play and is approximated through a simple circular, ecliptic ephemeris. This means that all planets are assumed to orbit the Sun in circular orbits (as holds in the CR3BP) and in the ecliptic plane, see Figure 3.

To describe the ephemerides, an inertial heliocentric reference frame is employed: the $\tilde{x}$-axis points towards the vernal equinox, the $\tilde{z}$-axis is perpendicular to the ecliptic plane and the $\tilde{y}$-axis completes the right-handed reference frame. In dimensional form, the ephemerides of the planets are then given by:

$$\tilde{\mathbf{r}}_P = \lambda \begin{bmatrix} \cos\left(\theta_0 + \dot{\theta}\tilde{t}_{\text{MJD2000, s}}\right) \\ \sin\left(\theta_0 + \dot{\theta}\tilde{t}_{\text{MJD2000, s}}\right) \\ 0 \end{bmatrix}, \quad \dot{\tilde{\mathbf{r}}}_P = \sqrt{\frac{\mu_S}{\lambda}} \begin{bmatrix} -\sin\left(\theta_0 + \dot{\theta}\tilde{t}_{\text{MJD2000, s}}\right) \\ \cos\left(\theta_0 + \dot{\theta}\tilde{t}_{\text{MJD2000, s}}\right) \\ 0 \end{bmatrix} \tag{5}$$

with $\dot{\theta} = 1/\tau$ and θ_0 the angular position of the planet at a reference epoch which is chosen to be 1-1-2000, similar to the mjd2000 notation. The time $\tilde{t}_{\text{MJD2000,s}}$ in Eq. (5) is the time in seconds after 1-1-2000 (i.e. $\tilde{t}_{\text{MJD2000,s}} = 0$ corresponds to 1-1-2000). The angular position of the planet at this reference epoch is calculated using the analytical ephemerides implemented in the Matlab® function *uplanet.m* [17] that was successfully verified against JPL/NAIF/SPICE de405 ephemerides.

Note that the assumption of circular, ecliptic ephemerides imposes little inaccuracies for Mars (eccentricity, $e = 0.093315$, and inclination, $i = 1.85$ deg), but introduces more significant errors for Mercury ($e = 0.205630$ and $i = 7.01$). However, the purpose of the current work is to demonstrate the feasibility of the concept. Future work will therefore consider more realistic and accurate planetary ephemerides.

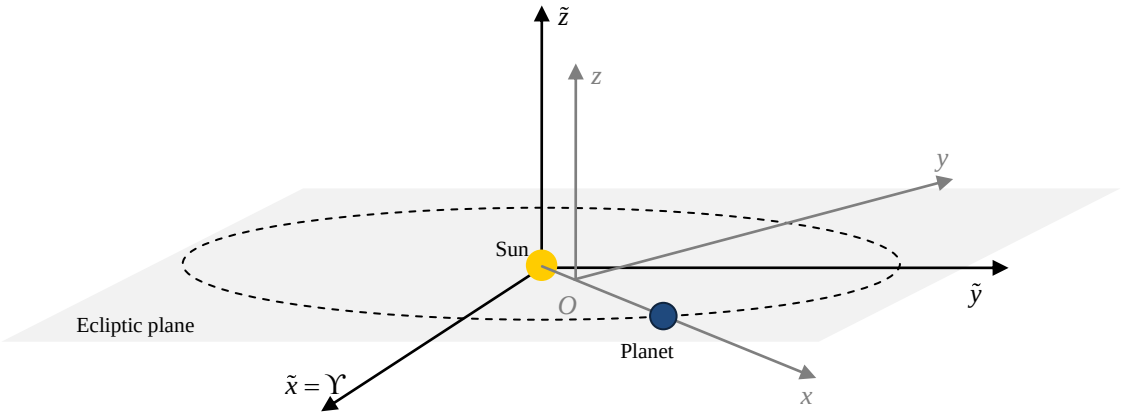

Figure 3 Schematic of circular ecliptic ephemeris of planets and definition of heliocentric inertial reference frame, $(\tilde{x}, \tilde{y}, \tilde{z})$, and Sun-planet synodic reference frame, (x, y, z).

Reference frame transformations

Since the ephemeris in Eq. (5) only provides the position and velocity of the fourth body in an heliocentric inertial reference frame, a transformation is required to obtain the planet's state vector in the Sun-planet synodic reference frame for use in Eq. (4).

The general transformation of a state vector $\tilde{\mathbf{x}} = \begin{bmatrix} \tilde{\mathbf{r}} & \dot{\tilde{\mathbf{r}}} \end{bmatrix}^T$ in the heliocentric inertial reference frame to a state vector $\mathbf{x} = \begin{bmatrix} \mathbf{r} & \dot{\mathbf{r}} \end{bmatrix}^T$ in the Sun-planet synodic reference frame is given through the following set of equations:

$$\theta = \tan 2^{-1}\left(\frac{\tilde{\mathbf{r}}_{P,y}}{\tilde{\mathbf{r}}_{P,\text{x}}}\right) \tag{6}$$

$$\mathbf{R}_z = \begin{bmatrix} \cos\theta & \sin\theta & 0 \\ -\sin\theta & \cos\theta & 0 \\ 0 & 0 & 1 \end{bmatrix} \tag{7}$$

$$\mathbf{r}' = \mathbf{R}_z \tilde{\mathbf{r}} \tag{8}$$

$$\begin{aligned} \dot{\mathbf{r}} &= \mathbf{R}_z \dot{\tilde{\mathbf{r}}} - \boldsymbol{\omega} \times \mathbf{r}' \\ \mathbf{r} &= \mathbf{r}' - \begin{bmatrix} \mu & 0 & 0 \end{bmatrix}^T \end{aligned} \tag{9}$$

where the matrix $\mathbf{R}_z$ rotates the $\tilde{x}$-axis of the heliocentric inertial reference frame onto the x-axis of the Sun-planet synodic reference frame and Eq. (9) accounts for the rotational velocity of the synodic reference frame and translates the origin from the Sun to the barycentre.

A simple relationship also exists between the dimensional time $\tilde{t}_{\text{MJD2000,s}}$ in the heliocentric inertial reference frame and the dimensionless time t in the Sun-planet synodic reference frame. By defining $t = \tilde{t}_{\text{MJD2000,s}} = 0$ to be 1-1-2000, $t = 2\pi$ corresponds to $\tilde{t}_{\text{MJD2000,s}} = 2\pi/\tau$, or equivalently: 1-1-2001 in the Sun-Earth problem, 18-11-2001 in the Sun-Mars problem and 29-3-2000 in the Sun-Mercury problem.

Lagrange Point Orbits

As discussed, when discarding the solar sail and fourth body perturbation accelerations in Eq. (1), the classical CR3BP is obtained. This problem generates five equilibrium solutions, or Lagrange points, by setting the time derivatives of the position vector equal to zero, i.e. $\ddot{\mathbf{r}} = \dot{\mathbf{r}} = 0$. The two Lagrange points considered in this work are the collinear L_1 (between m_1 and m_2) and L_2 (behind m_2) points. It is well-known that a range of periodic orbits can be found around these Lagrange points. Here the family of Halo orbits is considered and the method to generate these orbits can be found in Reference [18]. Four particular Halo orbits are selected, one around Earth-L_1, one around Earth-L_2, one around Mars-L_1 and one around Mercury-L_2. The projections onto the ecliptic and out-of-ecliptic plane for each of the Halo orbits are given in Figure 4, while Table 2 gives further details. Note that the Halo orbits in Figure 4 can be generated by simply forward integrating the initial conditions $\begin{bmatrix} \mathbf{r}_0 & \dot{\mathbf{r}}_0 \end{bmatrix}^T$ provided in Table 2 in Eq. (1) with $\mathbf{a}_s = \mathbf{a}_4 = \mathbf{0}$.

Table 2 Details of Halo orbits with $\mathbf{r}_0$ and $\dot{\mathbf{r}}_0$ the initial position and velocity vector and P_{LPO} the orbital period. Note that all variables are made dimensionless with respect to the *respective* CR3BP.

Halo orbit	$\begin{bmatrix} \mathbf{r}_0 & \dot{\mathbf{r}}_0 \end{bmatrix}^T$	P_{LPO}
Earth-L_2	$\begin{bmatrix} 1.0068 & 0 & -0.0035683 & 0 & 0.014705 & 0 \end{bmatrix}^T$	3.0741
Mars-L_1	$\begin{bmatrix} 0.99477 & 0 & -0.0016975 & 0 & 0.004996 & 0 \end{bmatrix}^T$	3.0602
Earth-L_1	$\begin{bmatrix} 0.9892 & 0 & -0.0048992 & 0 & 0.011603 & 0 \end{bmatrix}^T$	3.0388
Mars-L_2	$\begin{bmatrix} 1.0025 & 0 & 0.0014694 & 0 & 0.0059461 & 0 \end{bmatrix}^T$	3.0555

OPTIMISATION PROBLEM

With the initial and target LPOs defined, the problem now becomes to find optimal solar sail transfers between these LPOs. In particular between Earth-L_2 and Mars-L_1 and between Earth-L_1 and Mercury-L_2

In general, an optimal control problem can be defined as finding a state history $\mathbf{x}(t) \in \mathbb{R}^{n_x}$ and a control history $\mathbf{u}(t) \in \mathbb{R}^{n_u}$ with $t \in [t_0, t_f]$ the independent variable, that minimises a cost function, J. In this work, the cost function is the time of flight:

$$J = t_f - t_0 \tag{10}$$

where the subscripts 0 and f indicate the initial and final conditions, respectively.

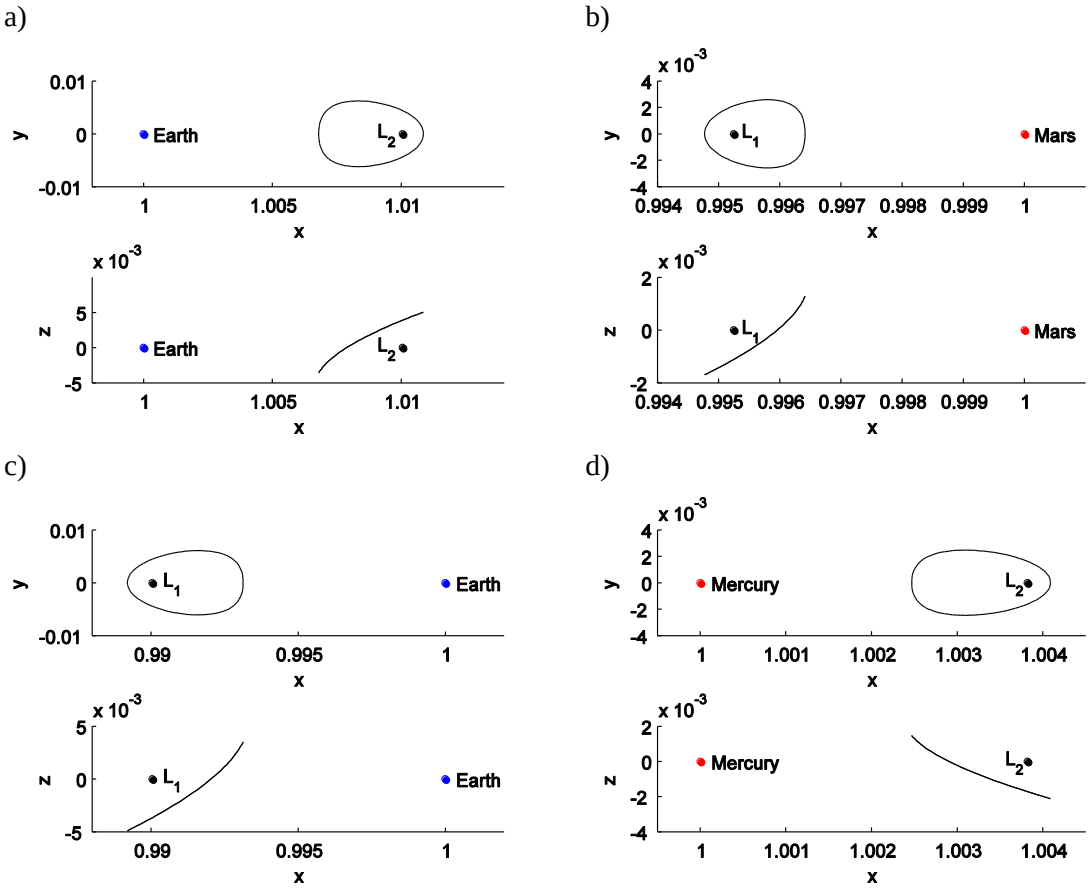

Figure 4 Projections of Halo orbits around: a) Earth-L_2 b) Mars-L_1 c) Earth-L_1 and d) Mercury-L_2.

The state history consists of the Cartesian position and velocity components in the Sun-planet synodic reference frame of Figure 1:

$$\mathbf{x} = [x \quad y \quad z \quad \dot{x} \quad \dot{y} \quad \dot{z}]^T \tag{11}$$

where the time dependency is omitted for ease of notation and appropriate bounds on these Cartesian position and velocity components are selected for each of the cases considered.

The control history consists of the Cartesian components of the normal vector to the solar sail (or equivalently the unit solar sail acceleration vector):

$$\begin{bmatrix}-1 & -1 & -1\end{bmatrix}^T \le \mathbf{u} = \begin{bmatrix}n_x & n_y & n_z\end{bmatrix}^T \le \begin{bmatrix}1 & 1 & 1\end{bmatrix}^T \tag{12}$$

Finally, the independent variable is the dimensionless time, t. Bounds on the initial and final time are imposed such that a 2020-2025 launch window and a 2020-2027 arrival window are ensured. In dimensionless time, these windows translate into:

$$\begin{aligned} 40\pi \le t_{0,} \le 50\pi \quad & \text{Sun-Earth system} \\ 21.2\pi \le t_f \le 28.8\pi \quad & \text{Sun-Mars system} \\ 166.1\pi \le t_f \le 224.2\pi \quad & \text{Sun-Mercury system} \end{aligned} \tag{13}$$

Two-phase approach

As indicated before, due to the fact that the initial and target LPOs are defined in different CR3BPs, the initial and final parts of the transfer will also have to be defined in different CR3BPs. The transfer is therefore split into two phases, where the first phase (hereafter referred to through the subscript p_1) is defined in the Sun-Earth CR3BP with either Mars of Mercury as fourth body, while the second phase (referred to through the subscript p_2) is defined in the Sun-Mars/Mercury CR3BP with Earth as fourth body, see also Figure 5.

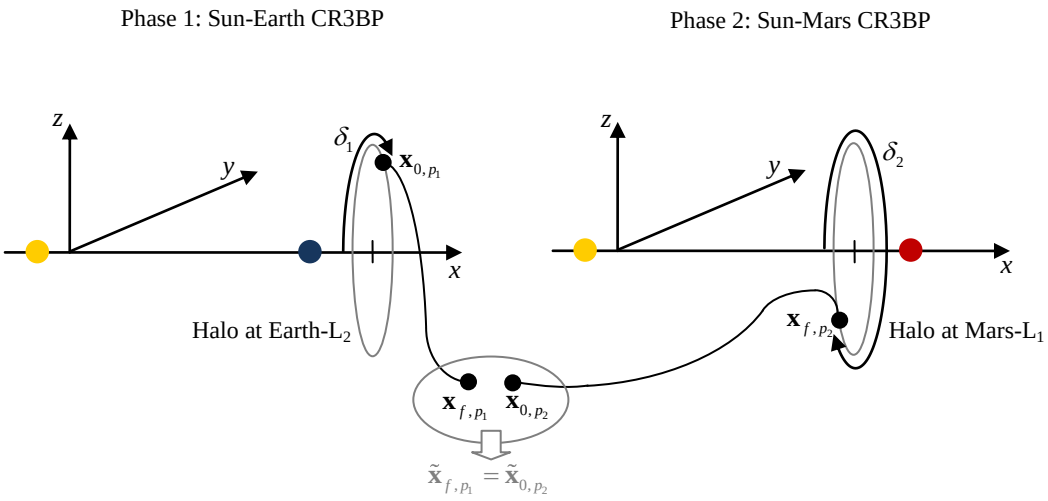

Figure 5 Illustration of two-phase approach for the Earth-L$_2$ to Mars-L$_1$ transfer and definition of static optimisation parameters δ_1 and δ_2.

Clearly, a smooth linkage between the two phases has to exist, i.e. a smooth linkage between the final conditions of the first phase and the initial conditions of the second phase. Therefore,

constraints are enforced that guarantee continuity across the linkage in terms of position, velocity, time and sail attitude. Since two different CR3BPs are linked, the relative orientation of the synodic reference frames at the time of the linkage needs to be considered. Therefore, the reverse of the transformation described in Eqs. (6)-(9) is used to transform the final state vector of the first phase, $\mathbf{x}_{f,p_1}$, and the initial state vector of the second phase, $\mathbf{x}_{0,p_2}$, to the heliocentric inertial reference frame. In this reference frame, the two state vectors can be equated to ensure a continuous link between the two phases:

$$\tilde{\mathbf{x}}_{f,p_1} = \tilde{\mathbf{x}}_{0,p_2} \tag{14}$$

A similar transformation is performed to obtain a continuous link on the sail attitude such that the following constraint can be enforced:

$$\tilde{\mathbf{u}}_{f,p_1} = \tilde{\mathbf{u}}_{0,p_2} \tag{15}$$

Finally, the dimensionless time is converted to dimensional time $\tilde{t}_{\text{MJD2000}}$ to also guarantee a continuous link in terms of time:

$$\tilde{\tilde{t}}_{\text{MJD2000},f,p_1} = \tilde{t}_{\text{MJD2000},0,p_2} \tag{16}$$

From Eqs. (14)-(16) it is clear that, in total, 10 linkage constraints are enforced.

Boundary constraints

To ensure that the trajectory departs from the Earth L_2/L_1 LPO and winds onto the Mars-L_1 or Mercury-L_2 LPO, a set of boundary constraints are imposed: the state vector at the start of phase 1, $\mathbf{x}_{0,p_1}$, should coincide with the Earth L_2/L_1 LPO and the state vector at the end of phase 2, $\mathbf{x}_{f,p_2}$, should coincide with the Mars-L_1 or Mercury-L_2 LPO. Two static optimisation parameters are used to find the optimum departure and arrival location on these LPOs. These static parameters are measured along the LPOs and are defined as $0 \le \delta_1 \le P_{LPO,p_1}$ and $0 \le \delta_2 \le P_{LPO,p_2}$, see also Figure 5 and Table 2 for values. The boundary constraints thus become:

$$\mathbf{x}_{0,p_1} = \mathbf{x}_{LPO,p_1}(\delta_1) \tag{17}$$

$$\mathbf{x}_{f,p_2} = \mathbf{x}_{LPO,p_2}(\delta_2) \tag{18}$$

The actual values for $\mathbf{x}_{LPO,p_1}(\delta_1)$ and $\mathbf{x}_{LPO,p_2}(\delta_2)$ are computed through an interpolation of large state matrices that provide the position and velocity vectors along the LPOs for a fine mesh in δ_1 or δ_2, i.e. for a discrete number of locations along each of the LPOs.

Note that no boundary constraints are imposed on the final conditions of the first phase and the initial conditions of the second phase. The choice for the location and time of the linkage as defined in Eqs. (14) and (16) are thus completely free and optimisable.

Path constraints

A set of path constraints are enforced on the control vector that will hold throughout the entire trajectory, i.e. in both phases 1 and 2. First, a path constraint is introduced to ensure that the norm of the control vector is unity:

$$|\mathbf{u}| = 1 \tag{19}$$

A second path constraint makes sure that the control vector always points away from the Sun. This has to be taken into account because a solar sail cannot generate an acceleration component in the direction of the Sun: [3]

$$\hat{\mathbf{r}}_1 \cdot \hat{\mathbf{n}} \geq 0 \tag{20}$$

A final path constraint is defined to introduce limitations on the control authority of the solar sail as discussed in the introduction of this paper. This is done by defining one more static optimisation parameter, $\frac{1}{2}\pi \leq \delta_3 \leq -\frac{1}{2}\pi$. This static parameter describes a constant cone angle, α_{ref}, to define an optimal solar sail reference attitude, $\hat{\mathbf{n}}_{\text{ref}}$, *in the ecliptic plane*, see Figure 6. To limit the control authority of the solar sail, the control vector $\mathbf{u}$ is now allowed to move within a cone around α_{ref} with a half-angle $\Delta\alpha$. The value for $\Delta\alpha$ is an input parameter of the optimal control problem. The associated path constraint then becomes:

$$\cos^{-1}\left(\hat{\mathbf{n}}_{\text{ref}} \cdot \hat{\mathbf{n}}\right) \leq \Delta\alpha \tag{21}$$

with $\hat{\mathbf{n}}_{\text{ref}} = \left[\cos\left(\gamma + \alpha_{\text{ref}}\right) \quad \sin\left(\gamma + \alpha_{\text{ref}}\right) \quad 0\right]^T$ and $\gamma = \tan 2^{-1}\left(y/\left(x + \mu\right)\right)$.

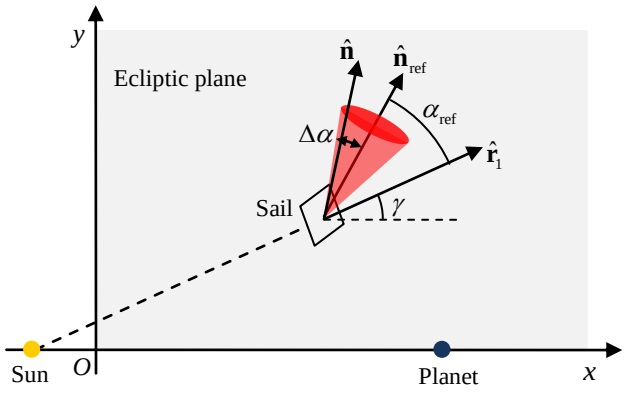

Figure 6 Illustration of solar sail limited control authority.

Optimal control solver

The optimal control problem defined in the previous sections is solved with a direct pseudospectral method, which discretises the time interval into a finite number of collocation points and uses Legendre or Chebyshev polynomials to approximate and interpolate the time dependent variables at the collocation points. This way, the infinite dimensional optimal control problem is transformed into a finite dimension non-linear programming (NLP) problem. Pseudospectral methods have become increasingly of interest for solving optimal control problems because the characteristics of the orthogonal polynomials are very well suited to the mathematical operations required to solve the optimal control problem: functions can be very accurately approximated, derivatives of the state functions at the nodes are computed by matrix multiplication only and any integral associated with the problem is approximated using well-known Gauss quadrature rules. This, together with the fact that pseudospectral methods have a rapid rate of convergence (i.e.

convergence to a very accurate solution with few number of nodes), is the reason for using pseudospectral methods in this work.

Here, a particular implementation of a direct pseudospectral method is chosen: PSOPT. [19] PSOPT is an open source tool developed by Victor M. Becerra of the University of Reading and is written in C++ and is interfaced to IPOPT (Interior Point OPTimizer) [20] to solve the NLP problem. PSOPT can deal with all optimal control problem elements defined above: multi-phase problems, phase linkage constraints, boundary constraints, path constraints, static optimisation parameters and bounds on state variables, control variables and time.

Initial guess

In order to initialise the optimisation, PSOPT requires an initial guess. Here, initial guesses for each of the transfer cases are generated using the concept of "patched restricted three-body problems approximation". [11, 21] Important to note is the fact that these initial guesses assume a constant attitude of the sail with respect to the Sun-sail line. They are sub-optimal in the sense that minor discontinuities exist in position and velocities at the linkage between the two three-body systems. By transferring these initial guesses into PSOPT and relieving the constraint on the constant sail attitude, feasible and time-optimal solutions are found.

The initial guesses are presented in Figure 7a for the Earth-L_2 to Mars-L_1 transfer and in Figure 7b for the Earth-L_1 to Mercury-L_2 transfer. While Figure 7a shows the transfer in the Sun-Earth synodic reference frame, Figure 7b uses the heliocentric inertial reference frame and also provides information on the solar sail acceleration vector through the use of arrows. As the size of the arrows indicate, the performance in terms of acceleration magnitude improves when the solar sail approaches Mercury, i.e. gets closer to the Sun where the photon irradiance and therefore solar sail acceleration is larger than at Earth distance.

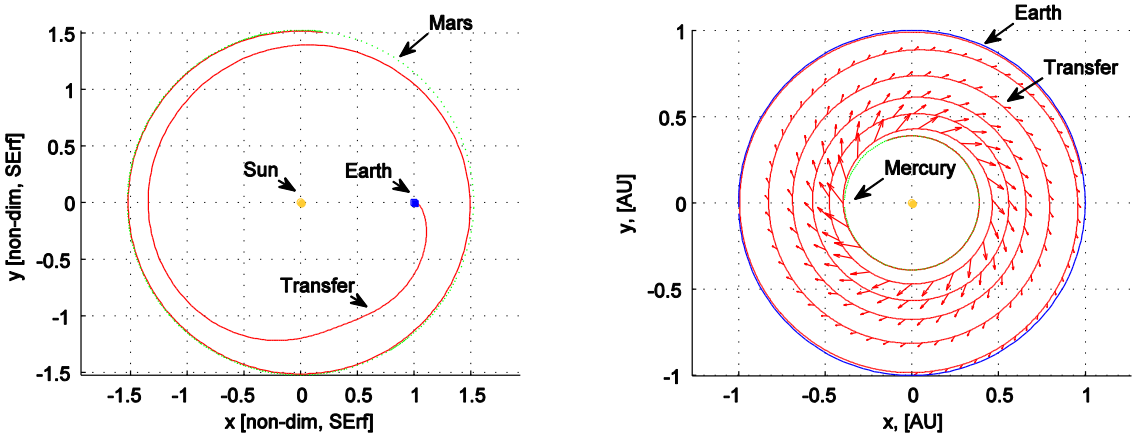

Figure 7 Initial guess trajectories. a) Earth-L_2 to Mars-L_1 transfer in Sun-Earth synodic reference frame. b) Earth-L_1 to Mercury-L_2 transfer in heliocentric inertial reference frame.

RESULTS – EARTH-L_2 TO MARS-L_1 TRANSFER

Using the initial guess shown in Figure 7a, a range of results for the Earth-L_2 to Mars-L_1 transfer are presented in this section. First, the results for a fully controllable sail are provided, where

the constraint in Eq. (21) is omitted. This will provide the absolute minimum time of flight achievable. Subsequently, the constraint in Eq. (21) is introduced and a continuation is started where the results for a larger value for $\Delta\alpha$ are used as an initial guess to obtain the results for a smaller value for $\Delta\alpha$. All results consist of 40 collocation points in both phases, i.e. 80 collocation points in total.

The main results are summarised in Table 3 for both the initial guess, the fully controllable solar sail (i.e. $\Delta\alpha$ is inactive) as well as for a range of values for $\Delta\alpha$. Figure 8 presents these results in graphical form to highlight the trend in the results. The smaller the value for $\Delta\alpha$, the more limited the controllability of the sail is. The table clearly demonstrates the effect of this limited controllability as the time of flight increases from 902 days for a fully controllable sail to 981 days for a very limited steering capability of $\Delta\alpha = 5$ deg. Despite this increase of 8.8 percent, it is remarkable that the transfer can be executed and all constraints can be satisfied with such limited control capabilities. Another effect of the decreasing value for $\Delta\alpha$ is an increase in the optimal reference sail attitude, α_{ref}. The solar sail acceleration direction thus becomes more tangential as the control capabilities decrease.

Table 3 Earth-L_2 to Mars-L_1 solar sail transfer results

Description	α_{ref}, deg	Departure date	Arrival date	Time of flight, days
Initial guess	n/a	11/11/2020	11/09/2026	2130
$\Delta\alpha$ inactive	n/a	19/01/2022	08/07/2024	902
$\Delta\alpha = 20$ deg	43.1	19/01/2022	13/07/2024	906
$\Delta\alpha = 15$ deg	43.9	20/01/2022	20/07/2024	913
$\Delta\alpha = 10$ deg	45.9	11/01/2022	31/07/2024	932
$\Delta\alpha = 7.5$ deg	47.9	28/12/2021	05/08/2024	950
$\Delta\alpha = 5$ deg	49.4	09/12/2021	15/08/2024	981

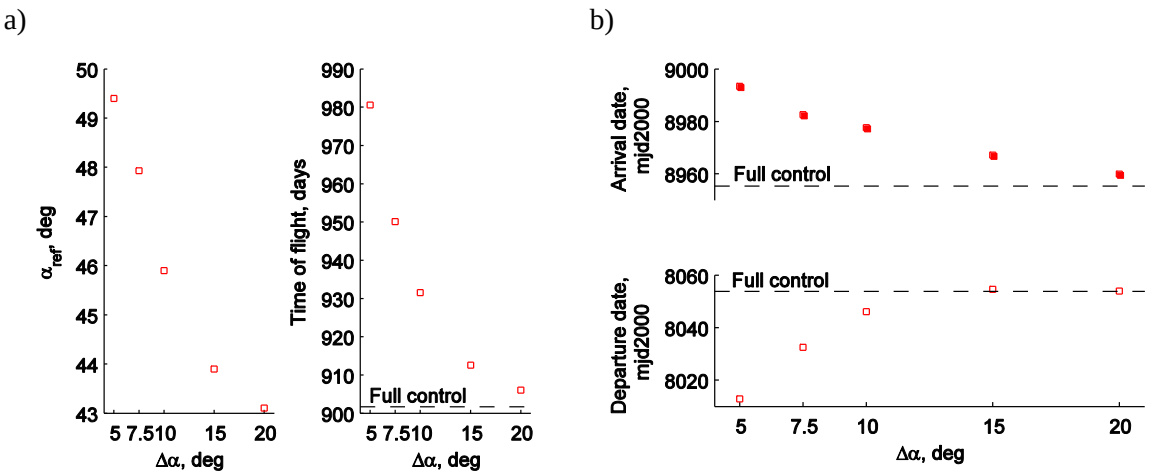

Figure 8 Earth-L_2 to Mars-L_1 solar sail transfers: influence of solar sail controllability, $\Delta\alpha$. a) Optimal sail reference attitude and time of flight. b) Departure and arrival times.

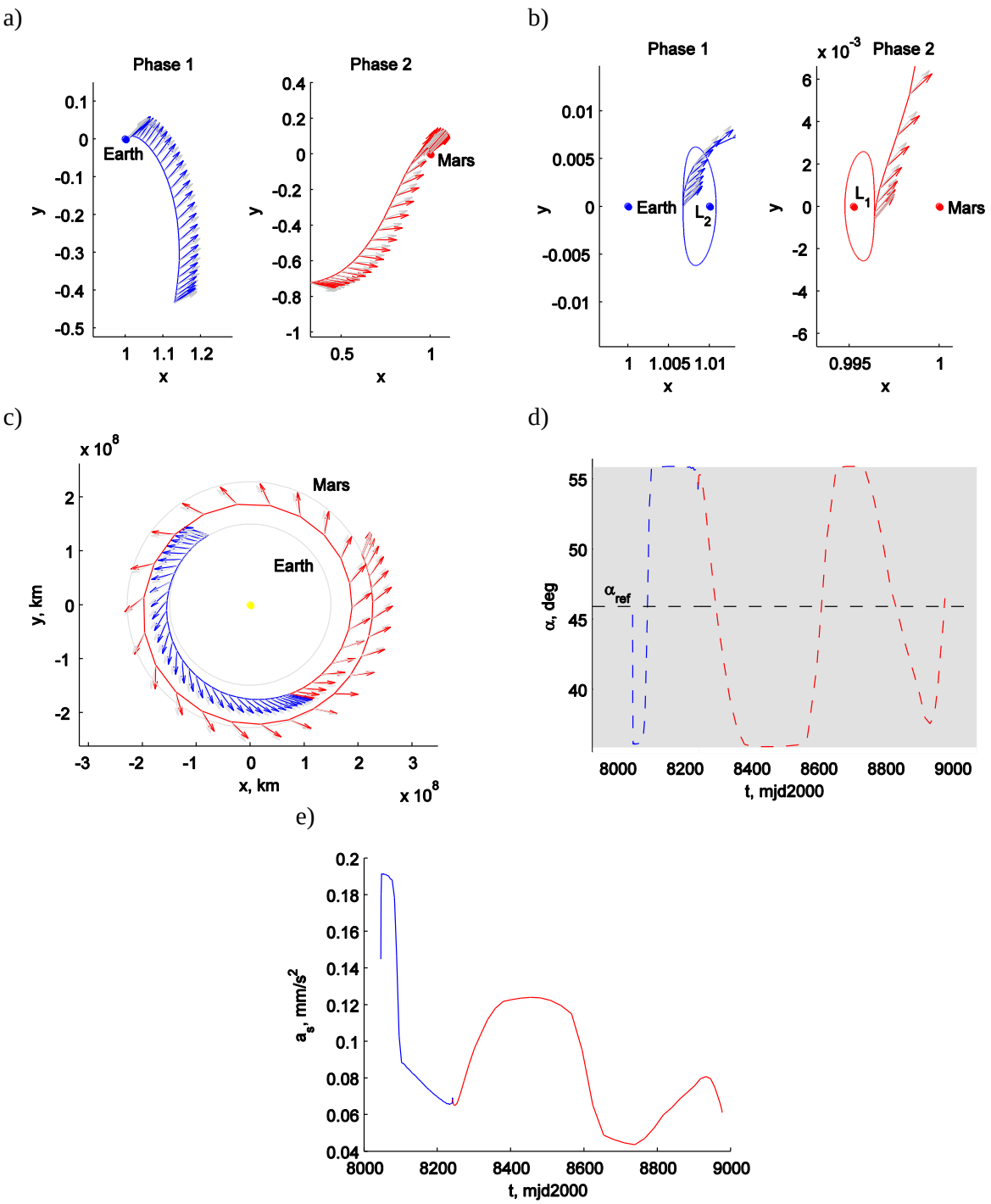

Figure 9 Earth-L_2 to Mars-L_1 solar sail transfer: details for $\Delta\alpha = 10$ deg. a) Transfer phases with sail acceleration direction (color) and optimal α_{ref} -direction (grey). b) Detail of plot a). c) Transfer in heliocentric inertial reference frame. d) Cone angle. e) Solar sail acceleration magnitude.

Note that the significant reduction in the time of flight between the initial guess and the fully controllable sail can be attributed to the fact that the initial guess considered coasting arcs at the start and end of the transfer while the time-optimal results presented here assume the use of the solar sail from the Earth-L_1 Halo orbit up to the Mars-L_2 Halo orbit.

Details of one particular transfer, i.e. for $\Delta\alpha =$ 10 deg are provided in Figure 9. The two phases of the problem are clearly indicated in all plots by distinguishing between the transfer leg in the Sun-Earth CR3BP in blue and the transfer leg in the Sun-Mars CR3BP in red. The optimal reference solar sail attitude is indicated with a grey arrow in plots a-c, while plot d shows the variation of the cone angle around this optimal reference attitude. The detail in Figure 9b shows where the transfer leaves the Earth-L_2 Halo and where it winds onto the Mars-L_1 Halo. The corresponding values for the optimisation parameters δ_1 and δ_2 are: $\delta_1 =$ 3.0741 and $\delta_2 =$ 1.6379, which closely corresponds to the intersection of the Halo orbits with the ecliptic plane. Very similar values for δ_1 and δ_2 are observed for other, small values for $\Delta\alpha$. This can most likely be attributed to the fact that the reference attitude of the solar sail is defined in the ecliptic plane. A small value for $\Delta\alpha$ therefore only allows very minor out-of-plane accelerations and as a consequence the trajectories will be almost entirely located in the ecliptic plane, including the locations where the sail departs from and winds onto the Halo orbits. Finally, in Figure 9e the solar sail acceleration magnitude is provided, which shows an expected decrease when the distance from the Sun becomes larger.

Comparison of the results with results in existing literature is difficult as the literature only considers solar sail orbital rendezvous missions to Mars [15, 22, 23]. In addition, different models are often used for the dynamics, the solar sail acceleration and/or the ephemerides. Although Reference [23] considers a time-free orbital rendezvous with Mars in a heliocentric two-body model, the ephemerides of Earth and Mars are the same as in this work: circular and in the ecliptic. Furthermore, an ideal solar sail model with $a_c = 1$ mm/s^2 (i.e. $\beta = 0.169$) is considered to obtain a minimum time of flight transfer of 408 days with an average cone angle of 44.94 deg for a fully controllable solar sail. Solving the problem considered in this work for a fully controllable solar sail and for $\beta = 0.169$, a minimum time of flight of 348 days is obtained with an average cone angle of 36.5 deg.

Limitations on the steering capabilities of the solar sail as introduced in this paper are only considered in Reference [15]. There, the authors fix the cone angle of the solar sail and allow only the clock angle to vary. Note that the cone angle restricts the solar sail acceleration vector to a cone around the Sun-sail line and the clock angle determines the location of the sail acceleration vector on this cone. In this case, due to differences in the assumed models (eccentricity and inclination of planets, optical solar sail force model), the minimum time of flight for the fully controllable sail is 381 days for $a_c = 1$ mm/s^2. The authors then find that a constant cone angle of 43 deg minimises the penalty on the time of flight, which becomes 405 days. It is clear that a constant cone angle of 43 deg and a clock angle variation between $-\pi$ and π still provides much more control capabilities to the sail than the restrictions imposed in this work: results for $\Delta\alpha$-values down to 10 deg have been obtained for which the time of flight increases to 560 days. Interestingly, this is a much larger percentage increase (61 percent) than for a sail performance of $\beta =$ 0.05 as considered in Table 3 and Figure 8. Furthermore, feasible trajectories were not found for $\Delta\alpha < 10$ deg, while for $\beta =$ 0.05 trajectories were found for $\Delta\alpha$-values down to 5 deg. It therefore seems that the limitations on the sail steering capabilities have a larger impact for better sail performances.

RESULTS – EARTH-L_1 TO MERCURY-L_2 TRANSFER

The optimal results for the Earth-L_1 to Mercury-L_2 transfer are presented in a similar way as for the Earth-L_2 to Mars-L_1 transfer: Table 4 provides departure and arrival dates and time of flight for the initial guess, the fully controllable solar sail and for different values for $\Delta\alpha$. It also contains the optimal reference attitude of the solar sail, α_{ref}. Figure 10 provides similar information in graphical form, while Figure shows details of the transfer with $\Delta\alpha =$ 2.5 deg.

Very similar conclusions as for the Earth-Mars transfer can be drawn for the Earth-Mercury transfer: the smaller the value for $\Delta\alpha$, the larger the time of flight and the larger the value for α_{ref} although for $\Delta\alpha =$ 2.5 deg a slightly larger α_{ref} appeared advantageous. Considering the penalty on the time of flight for decreasing $\Delta\alpha$, it becomes clear that this penalty is only very minor for the Earth-Mercury transfer: 763 days for a fully controllable solar sail and 778 days for $\Delta\alpha =$ 2.5 deg, which is an increase of only 2.0 percent. Furthermore, from Table 4 and Figure 11 it becomes clear that the Earth-Mercury transfer can be achieved with even less control authority than the Earth-Mars transfer: even for $\Delta\alpha =$ 2.5 deg an optimal trajectory is found with $\delta_1 = 1.3506$ and $\delta_2 = 2.1717$.

Table 4 Earth-L_1 to Mercury-L_2 solar sail transfer results

Description	α_{ref}, deg	Departure date	Arrival date	Time of flight, days
Initial guess	n/a	02/10/2020	30/03/2024	1269.4
$\Delta\alpha$ inactive	n/a	14/10/2021	16/11/2023	763
$\Delta\alpha = 10$ deg	-40.7	14/10/2021	16/11/2023	763
$\Delta\alpha = 7.5$ deg	-39.7	13/10/2021	16/11/2023	764
$\Delta\alpha = 5$ deg	-38.4	12/10/2021	18/11/2023	767
$\Delta\alpha = 2.5$ deg	-40.4	06/10/2021	23/11/2023	778

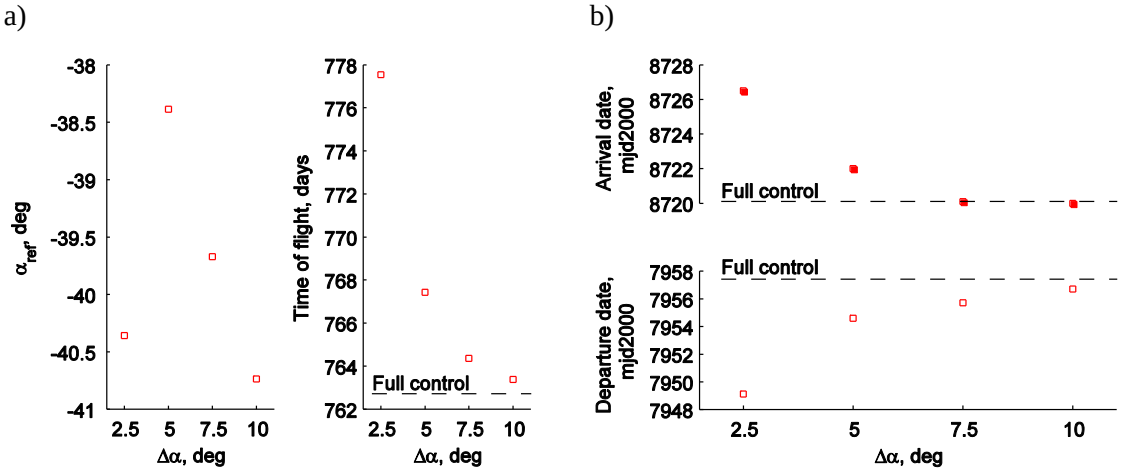

Figure 10 Earth-L_1 to Mercury-L_2 solar sail transfers: influence of solar sail controllability, $\Delta\alpha$. a) Optimal sail reference attitude and time of flight. b) Departure and arrival times.

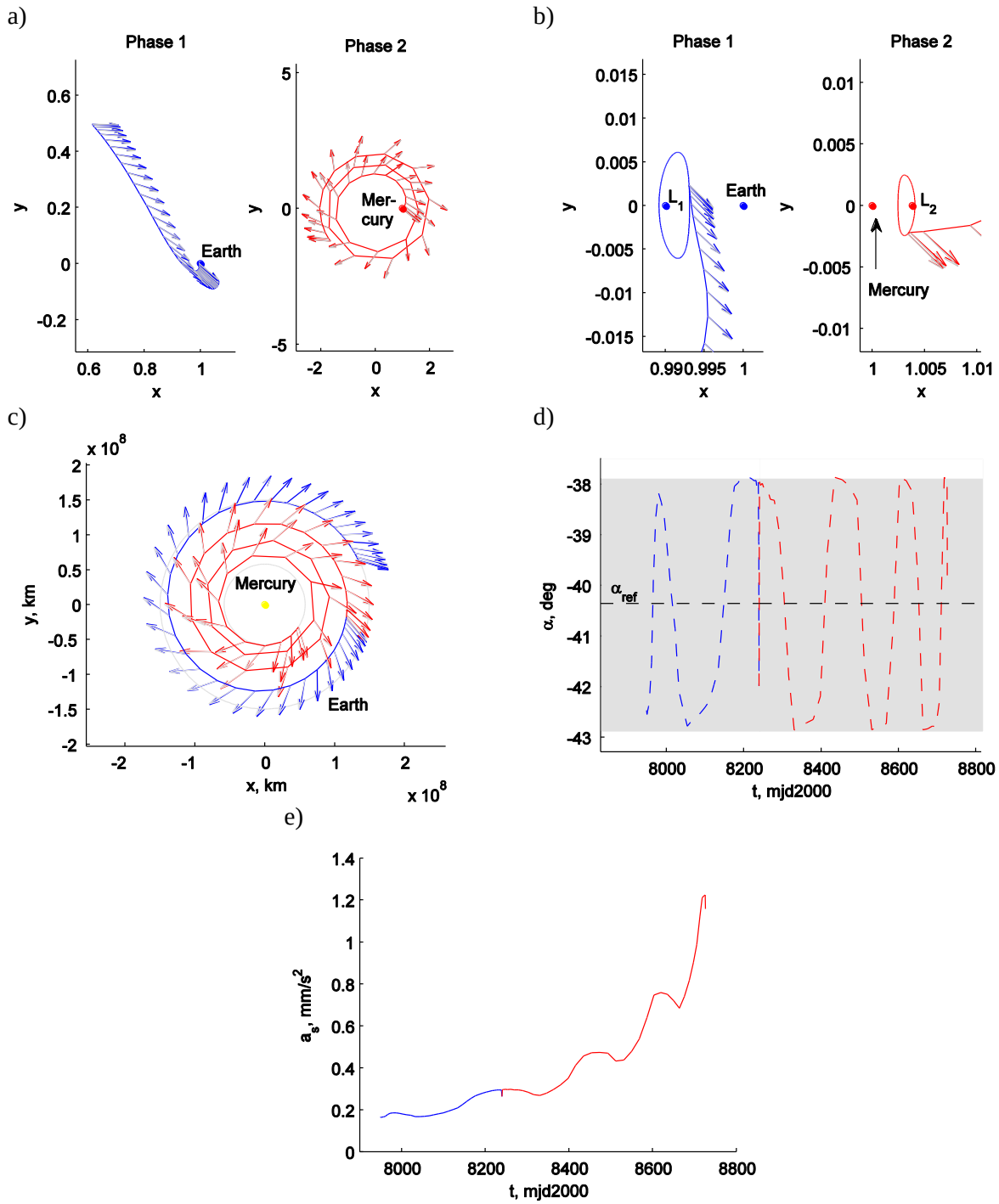

Figure 11 Earth-L_1 to Mercury-L_2 solar sail transfer: details for $\Delta\alpha = 2.5$ deg. a) Transfer phases with sail acceleration direction (color) and optimal α_{ref}-direction (grey). b) Detail of plot a). c) Transfer in heliocentric inertial reference frame. d) Cone angle. e) Solar sail acceleration magnitude.

A comparison with existing results in the literature is again difficult due to differences in dynamical and solar sail models and ephemerides. However, Reference [24] does provide a minimum time of flight for the fully controllable sail between co-planar circular Earth and Mercury orbits. However, an optical sail model and an orbital rendezvous rather than a transfer between LPOs of different CR3BP is considered. The result in Reference [24] for a characteristic sail acceleration of 0.3 mm/s^2 is 2.4 years or approximately 875 days, which is significantly larger than the time of flights in Table 4.

CONCLUSIONS

In this paper, optimal solar sail trajectories between displaced Libration Point Orbits (LPOs) of different restricted three-body systems have been investigated. Two transfers have been considered in particular: 1) from an Earth-L_2 Halo orbit to a Mars-L_1 Halo orbit and 2) from an Earth-L_1 Halo orbit to a Mercury-L_2 Halo orbit. In addition, the paper has focused on finding transfers that are achievable both with fully controllable solar sails as well as with low control authority solar sails (mimicking the capabilities of SpaceChips). In all cases, the objective has been to minimise the time of flight. To that end, the optimal control problem has been derived and solved with a particular implementation of a direct pseudospectral method, PSOPT. A two-phase approach has been adopted in order to model the start of the transfer in one CR3BP and the end of the transfer in another CR3BP (including fourth body perturbations). These phases are linked in terms of state, control and time in inertial space considering circular, ecliptic ephemerides for the planets involved. The case of low control authority solar sails is modeled by defining a cone of half angle $\Delta\alpha$ around a to-be optimised reference attitude. The results show that, for a sail performance comparable to that of NASA's Sunjammer sail, the Earth-Mars and Earth-Mercury transfers can be performed with very little steering effort as $\Delta\alpha$ can be as small as 5 deg and 2.5 deg, respectively. Compared to a fully controllable solar sail, the penalty on the time of flight is modest: for the Earth-Mars transfer, the transfer times are 902 days (full control) and 981 days ($\Delta\alpha = 5$ deg), while for the Earth-Mercury transfer, the transfer times are 763 days (full control) and 778 days ($\Delta\alpha = 2.5$ deg), all within a 2020-2025 launch window and 2020-2027 arrival window. When increasing the sail performance it seems that the penalty on the time of flight increases and that the control capabilities cannot be as limited (in terms of the minimum value for $\Delta\alpha$) as for less performance sails.

ACKNOWLEDGEMENTS

This work was funded by the European Research Council Advanced Investigator Grant-227571: Visionary Space Systems: Orbital Dynamics at Extremes of Spacecraft Length-Scale.

REFERENCES

1. Tsuda, Y., Mori, O., Funase, R., Sawada, H., Yamamoto, T., Saiki, T., Endo, T., and Kawaguchi, J. "Flight Status of IKAROS Deep Space Solar Sail Demonstrator," *Acta Astronautica* Vol. 69, No. 9-10, 2011, pp. 833-840. doi: 10.1016/j.actaastro.2011.06.005

2. L'Garde Inc. "L'Garde - Sunjammer." http://www.lgarde.com/programs/space-propulsion/sunjammer, Accessed 8 May 2013.

3. McInnes, C. R. *Solar Sailing: Technology, Dynamics and Mission Applications*. Berlin: Springer-Praxis Books in Astronautical Engineering, Springer-Verlag, 1999.

4. Heiligers, J., Ceriotti, M., McInnes, C. R., and Biggs, J. D. "Displaced Geostationary Orbit Design Using Hybrid Sail Propulsion," *Journal of Guidance, Control, and Dynamics* Vol. 34, No. 6, 2011, pp. 1852-1866. doi: 10.2514/1.53807

5. Baig, S., and McInnes, C. R. "Light-Levitated Geostationary Cylindrical Orbits Are Feasible," *Journal of Guidance, Control, and Dynamics* Vol. 33, No. 3, 2010, pp. 782-793. doi: 10.2514/1.46681

6. Wawrzyniak, G. G., and Howell, K. C. "Investigating the Design Space for Solar Sail Trajectories in the Earth-Moon System," *The Open Aerospace Engineering Journal* Vol. 4, 2011, pp. 26-44.

7. McInnes, C. R. "Solar Sail Trajectories at the Lunar L2 Lagrange Point," *Journal of Spacecraft and Rockets* Vol. 30, No. 6, 1993, pp. 782-784. doi: 10.2514/3.26393

8. Heiligers, J., Ceriotti, M., and McInnes, C. R. "Hybrid low-thrust transfers to eight-shaped orbits for polar observation (IAC-12-C.1.4.2)," *63rd International Astronautical Congress*. Naples, Italy, 2012.

9. Heiligers, J., and McInnes, C. R. "Agile Solar Sailing in Three-body Problem: Motion Between Artificial Equilibrium Points (IAC-13-C1.8.3)," *64th International Astronautical Congress*. Beijing, China, 2013.

10. Pergola, P., Geurts, K., Casaregola, C., and Andrenucci, M. "Earth-Mars Halo to Halo Low Thrust Manifold Transfers," *Celestial Mechanics and Dynamical Astronomy* Vol. 105, 2009, pp. 19-32. doi: 10.1007/s10569-009-9205-6

11. Mingotti, G., Topputo, F., and Bernelli-Zazzera, F. "Earth–Mars transfers with ballistic escape and low-thrust capture," *Celestial Mechanics and Dynamical Astronomy* Vol. 110, No. 2, 2011, pp. 169-188. doi: 10.1007/s10569-011-9343-5

12. Topputo, F., Vasile, M., and Bernelli-Zazzera, F. "Low Energy Interplanetary Transfers Exploiting Invariant Manifolds of the Restricted Three-Body Problem," *Journal of the Astronautical Sciences* Vol. 53, 2005, pp. 353-372.

13. Baoyin, H., and McInnes, C. "Solar Sail Halo Orbits at the Sun-Earth Artificial L1-point," *Celestial Mechanics and Dynamical Astronomy* Vol. 94, 2006, pp. 155-171. doi: 10.1007/s10569-005-4626-3

14. Colombo, C., Lucking, C., and McInnes, C. "Orbital dynamics of high area-to-mass ratio spacecraft with J2 and solar radiation pressure for novel Earth observation and communication services," *Acta Astronautica* Vol. 81, 2012, pp. 137-150. doi: 10.1016/j.actaastro.2012.07.009

15. Mengali, G., and Quarta, A. A. "Optimal Solar Sail Interplanetary Trajectories with Constant Cone Angle," *Advances in Solar Sailing*. Springer-Praxis Books in Astronautical Engineering, Springer-Verlag, Berlin, 2014.

16. Battin, R. H. *An Introduction to the Mathematics and Methods of Astrodynamics, Revised Edition*. Reston, USA: American Institute of Aeronautics and Astronautics, Inc., 1999.

17. Dysli, P. "Analytical Ephemeris for Planets (MATLAB code uplanet.m)." 1977.

18. Howell, K. C. "Three-Dimensional, Periodic, 'Halo' Orbits," *Celestial Mechanics and Dynamical Astronomy* Vol. 32, 1983, pp. 53-71.

19. Becerra, V. M. "Solving Complex Optimal Control Problems at No Cost with PSOPT," *IEEE Multi-conference on Systems and Control*. Yokohama, Japan, 2010.

20. Wächter, A., and Biegler, L. T. "On the Implementation of an Interior-point Filter Line-search Algorithm for Large-scale Nonlinear Programming," *Mathematical Programming* Vol. 106, No. 1, 2006, pp. 25-57. doi: 10.1007/s10107-004-0559-y

21. Mingotti, G., Heiligers, J., and McInnes, C. R. "First-Guess Generation of Solar Sail Interplanetary Heteroclinic Connections," *2nd IAA Conference on Dynamics and Control of Space Systems*. Rome, Italy, 2014.

22. Circi, C. "Mars and Mercury Missions Using Solar Sails and Solar Electric Propulsion," *Journal of Guidance, Control, and Dynamics* Vol. 27, No. 3, 2004, pp. 496-498.

23. Mengali, G., and Quarta, A. A. "Solar Sail Trajectories with Piecewise-Constant Steering Laws," *Aerospace Science and Technology* Vol. 13, 2009, pp. 431-441.

24. Quarta, A. A., and Mengali, G. "Solar Sail Missions to Mercury with Venus Gravity Assist," *Acta Astronautica* Vol. 65, 2008, pp. 495-506.